Journal of Power Sources 241 (2013) 522–528

Contents lists available at SciVerse ScienceDirect

Journal of Power Sources

journal homepage: www.elsevier.com/locate/jpowsour

Synthesis and characterization of $xLi_2MnO_3 \cdot (1-x)LiMn_{1/3}Ni_{1/3}Co_{1/3}O_2$ composite cathode materials for rechargeable lithium-ion batteries

Ozan Toprakci [1], Hatice A.K. Toprakci [1], Ying Li [1], Liwen Ji [1], Leigang Xue, Hun Lee, Shu Zhang, Xiangwu Zhang*

Fiber and Polymer Science Program, Department of Textile Engineering, Chemistry and Science, North Carolina State University, 2401 Research Drive, Raleigh, NC 27695-8301, USA

HIGHLIGHTS

- $xLi_2MnO_3 \cdot (1-x)LiMn_{1/3}Ni_{1/3}Co_{1/3}O_2$ composite cathode materials were prepared by a single-step sol–gel technique.
- Deionized water was used as solvent.
- $0.3Li_2MnO_3 \cdot 0.7LiMn_{1/3}Ni_{1/3}Co_{1/3}O_2$ composite showed the best electrochemical performance.
- Initial discharge capacity of 186 mAh g^{-1} was obtained at 0.1C.

ARTICLE INFO

Article history:
Received 31 January 2013
Received in revised form
24 April 2013
Accepted 30 April 2013
Available online 13 May 2013

Keywords:
Lithium-ion batteries
Cathodes
Electrochemical performance
Li-rich
$xLi_2MnO_3 \cdot (1-x)LiCo_{1/3}Ni_{1/3}Mn_{1/3}O_2$

ABSTRACT

Various $xLi_2MnO_3 \cdot (1-x)LiCo_{1/3}Ni_{1/3}Mn_{1/3}O_2$ (x = 0.1, 0.2, 0.3, 0.4, and 0.5) cathode materials were prepared by the one-step sol–gel route. The structure of $xLi_2MnO_3 \cdot (1-x)LiCo_{1/3}Ni_{1/3}Mn_{1/3}O_2$ composites was determined by X-ray diffraction analysis. The surface morphology and microstructure of $xLi_2MnO_3 \cdot (1-x)LiCo_{1/3}Ni_{1/3}Mn_{1/3}O_2$ composites were characterized using scanning electron microscopy and transmission electron microscopy. Electrochemical performance of $xLi_2MnO_3 \cdot (1-x)LiCo_{1/3}Ni_{1/3}Mn_{1/3}O_2$ composites was evaluated in terms of capacity, cycling performance and rate capability. Although the morphology and structure were found to be affected by the Li_2MnO_3 content, all composites showed an α-$NaFeO_2$ structure with R3m space group. Electrochemical results showed that cells using $0.3Li_2MnO_3 \cdot 0.7LiCo_{1/3}Ni_{1/3}Mn_{1/3}O_2$ composites had good performance, in terms of large reversible capacity, prolonged cycling stability, and excellent rate capability.

© 2013 Elsevier B.V. All rights reserved.

1. Introduction

Li-ion batteries (LIBs) are being widely used for mobile electronics because of their high energy storage capacity and excellent rechargeability [1–3]. LIBs became commercially available with the incorporation of lithium cobalt oxide ($LiCoO_2$) into the market by Sony in 1991. Although two decades pasted, $LiCoO_2$ is still the most used cathode material because of easy synthesis, relatively good cyclic stability and stable discharge voltage. On the other hand, $LiCoO_2$ is toxic, costly and has some safety issues. In addition, the energy density of $LiCoO_2$ is not sufficient for the electrical vehicle (EV) application since only half of its theoretical capacity can be achieved in practice due to the structural instability [1–3].

In order to minimize these problems, research efforts were initially focused on the substation of $LiCoO_2$ with lithium manganese dioxide ($LiMnO_2$) and lithium nickel oxide ($LiNiO_2$) because of their lower cost, better safety and higher abundance in nature [1–4]. Although $LiMnO_2$ has the advantages of high safety and low cost, interaction of Mn with the electrolyte and poor cycling stability at high temperatures are major obstacles for its commercial use in LIBs [3]. Similar with $LiMnO_2$, the use of $LiNiO_2$ in commercial LIBs is also hindered due to its cyclic instability, thermal instability, and low safety [3,5,6].

Recently, by taking consideration of the advantages and disadvantages of these three abovementioned cathode materials, research focus has been shifted to mixed forms of layered lithium metal (Li–Ni–Mn–Co) oxides [7–9]. These new cathodes offer

* Corresponding author. Tel.: +1 919 515 6547; fax: +1 919 515 6532.
E-mail address: xiangwu_zhang@ncsu.edu (X. Zhang).
[1] These authors contributed equally to this work.

0378-7753/$ – see front matter © 2013 Elsevier B.V. All rights reserved.
http://dx.doi.org/10.1016/j.jpowsour.2013.04.155

noticeable improvement in the capacity and cycling behavior [10,11]. Among all Li–Ni–Mn–Co based cathode materials, $LiNi_{1/3}Co_{1/3}Mn_{1/3}O_2$ attracted significant attention because of its good electrochemical properties such as high capacity, prolonged cycling life, and so on [8]. However, this material still has drawbacks such as structural and thermal instabilities. To address this, researchers have recently developed layered Li-rich composite materials such as $xLi_2MnO_3\cdot(1-x)LiCo_{1/3}Ni_{1/3}Mn_{1/3}O_2$ [12–19].

In $xLi_2MnO_3\cdot(1-x)LiCo_{1/3}Ni_{1/3}Mn_{1/3}O_2$ composites, the Li_2MnO_3 component can supply extra Li^+ ions at voltages higher than 4.5 V (leading to increased operational voltage) and increase the structural and thermal stabilities [16,20–23]. However, due to the composite-like structure, the electrochemical performance of $xLi_2MnO_3\cdot(1-x)LiCo_{1/3}Ni_{1/3}Mn_{1/3}O_2$ is directly affected by the process and composition of the material. Therefore, it is critical to determine the optimum combination in a given material preparation route. In the literature, optimum $xLi_2MnO_3\cdot(1-x)LiCo_{1/3}Ni_{1/3}Mn_{1/3}O_2$ compositions were obtained by using different production routes such as co-precipitation [15], molten salt techniques [24] etc. However, these techniques require extra washing, filtration, and grinding steps which increase the production cost and are also time-consuming. In this study, we prepared $xLi_2MnO_3\cdot(1-x)LiCo_{1/3}Ni_{1/3}Mn_{1/3}O_2$ ($x = 0.1, 0.2, 0.3, 0.4, 0.5$) composite materials with different compositions by a one-step sol–gel route. The one-step method is simple and can be easily scaled up for industrial production. Morphology, structure and electrochemical behavior of the prepared cathode materials were evaluated using different analytic techniques. Results show that with carefully controlled composition and structure, the prepared $xLi_2MnO_3\cdot(1-x)LiCo_{1/3}Ni_{1/3}Mn_{1/3}O_2$ can present excellent electrochemical performance in terms of large capacity, extended cycle life, and high rate capability. The improved electrochemical performance together with the low cost nature and simple preparation approach make it possible for using these new $xLi_2MnO_3\cdot(1-x)LiMn_{1/3}Ni_{1/3}Co_{1/3}O_2$ composite materials as promising cathode candidate in lithium-ion batteries.

2. Materials and method

2.1. Preparation of cathode materials

Various cathode composite materials $xLi_2MnO_3\cdot(1-x)LiCo_{1/3}Ni_{1/3}Mn_{1/3}O_2$ with different stoichiometric ratios ($x = 0.1, 0.2, 0.3, 0.4$, and 0.5) were prepared by a one-step sol–gel method. Fig. 1 shows the preparation procedure of $xLi_2MnO_3\cdot(1-x)LiCo_{1/3}Ni_{1/3}Mn_{1/3}O_2$ composites. Precursors lithium acetate ($LiCOOCH_3$, 99.99%, Sigma–Aldrich), manganese (II) acetate ($Mn(COOCH_3)_2$, 98%, Sigma–Aldrich), nickel (II) acetate tetrahydrate ($Ni(COOCH_3)_2\cdot4H_2O$, 99.998%, Sigma–Aldrich) and cobalt (II) acetate tetrahydrate ($Co(COOCH_3)_2\cdot4H_2O$, 97%, Acros Organics) with different ratios were added in deionized water and were mixed for 6 h. The total precursor concentration in all prepared solutions was fixed at 20 wt %. After mixing, samples were dried at 120 °C for 6 h and then calcined at 900 °C for 10 h. Table 1 shows the stoichiometric ratios of the acetate precursors used during the sample preparation and the theoretical capacities of the resultant $xLi_2MnO_3\cdot(1-x)LiCo_{1/3}Ni_{1/3}Mn_{1/3}O_2$ composites.

Table 1
Stoichiometric precursor ratios and the corresponding theoretical capacities of $xLi_2MnO_3\cdot(1-x)LiMn_{1/3}Ni_{1/3}Co_{1/3}O_2$ composites.

Chemical formula	Li acetate	Co acetate	Ni acetate	Mn acetate	Theoretical capacity (mAh g^{-1})
$0.1Li_2MnO_3\cdot0.9LiCo_{1/3}Ni_{1/3}Mn_{1/3}O_2$	1.1	0.30	0.30	0.40	299
$0.2Li_2MnO_3\cdot0.8LiCo_{1/3}Ni_{1/3}Mn_{1/3}O_2$	1.2	0.26	0.26	0.46	320
$0.3Li_2MnO_3\cdot0.7LiCo_{1/3}Ni_{1/3}Mn_{1/3}O_2$	1.3	0.23	0.23	0.53	340
$0.4Li_2MnO_3\cdot0.6LiCo_{1/3}Ni_{1/3}Mn_{1/3}O_2$	1.4	0.20	0.20	0.60	359
$0.5Li_2MnO_3\cdot0.5LiCo_{1/3}Ni_{1/3}Mn_{1/3}O_2$	1.5	0.16	0.16	0.66	377

2.2. Structural and morphological characterization

The structural characterization of $xLi_2MnO_3\cdot(1-x)LiCo_{1/3}Ni_{1/3}Mn_{1/3}O_2$ composites was carried out by small-angle X-ray diffraction (SAXD, Rigaku Smartlab X-ray Diffraction System, Cu Kα, $\lambda = 1.5405$ Å) in a 2θ range of $5-90°$, with 2θ step-scan intervals of 0.05°. The morphology and particle size distribution of the composites were evaluated by using field emission scanning electron microscope (FESEM–JEOL 6400F SEM at 5 kV). The microstructure was also observed using transmission electron microscope (Hitachi HF2000 TEM at 200 kV). Before TEM observation, composites were ultrasonically treated in a solution of ethanol and then deposited on 200-mesh carbon-coated copper grids.

2.3. Electrochemical measurements

Electrodes were prepared by mixing of 80 wt % active material, 10 wt % carbon black (Ketjen Black, Akzo Nobel), and 10 wt % poly(vinylene difluoride) (PVDF, 1,300,000 g mol^{-1}, Acros Organics) in 1-methyl-2-pyrrolidone (NMP, Aldrich). The obtained slurry was casted on aluminum foil and dried in a vacuum oven at 115 °C for 24 h. CR2032-type coin cells (diameter = 20 mm and height = 3.2 mm) were fabricated by using lithium metal as the counter electrode in an argon-filled glove box. The cathode weight was around 4 mg per electrode. The electrolyte used consisted of 1 M solution of $LiPF_6$ in a mixture (1:1:1 by volume) of ethylene carbonate (EC), dimethyl carbonate (DMC) and diethyl carbonate (DEC). The separator (Celgard 2400) was soaked in the electrolyte

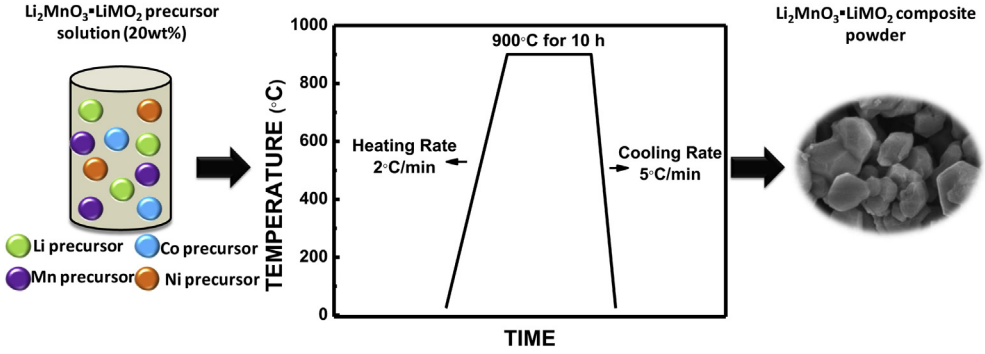

Fig. 1. Schematic diagram of preparation $xLi_2MnO_3\cdot(1-x)LiMn_{1/3}Ni_{1/3}Co_{1/3}O_2$ composite cathode materials for lithium-ion batteries.

for 24 h prior to testing. Coin-cells were galvanostatically charged/discharged on Arbin BT2000 battery cycler at various current densities (where 1C = 299 mA g^{-1} for $0.1Li_2MnO_3{\cdot}0.9LiMn_{1/3}Ni_{1/3}Co_{1/3}O_2$, 1C = 320 mA g^{-1} for $0.2Li_2MnO_3{\cdot}0.8LiMn_{1/3}Ni_{1/3}Co_{1/3}O_2$, 1C = 340 mA g^{-1} for $0.3Li_2MnO_3{\cdot}0.7LiMn_{1/3}Ni_{1/3}Co_{1/3}O_2$, 1C = 359 mA g^{-1} for $0.4Li_2MnO_3{\cdot}0.6LiMn_{1/3}Ni_{1/3}Co_{1/3}O_2$, and 1C = 377 mA g^{-1} for $0.5Li_2MnO_3{\cdot}0.5LiMn_{1/3}Ni_{1/3}Co_{1/3}O_2$).

Electrochemical impedance spectra (EIS) measurements were performed using a frequency response analyzer (Gamry Reference 600 Potentiostat) in a frequency range of 1 MHz–1 mHz and a potentiostatic signal amplitude of 10 mV s^{-1}. All electrochemical experiments were conducted at room temperature.

3. Results and discussion

3.1. Structure of $xLi_2MnO_3{\cdot}(1-x)LiNi_{1/3}Co_{1/3}Mn_{1/3}O_2$ composites

The XRD patterns of $xLi_2MnO_3{\cdot}(1-x)LiCo_{1/3}Ni_{1/3}Mn_{1/3}O_2$ ($x = 0.1, 0.2, 0.3, 0.4$, and 0.5) are shown in Fig. 2. All five composites show a hexagonal α-$NaFeO_2$ structure with R3m space group, which is an indication of alternating layers of Li, Ni, Mn, Co in a single phase layered structure [15,19,25]. Crystallite sizes of the composites were calculated by Scherrer's equation and were found to be 102, 146, 187, 192 and 204 nm for $xLi_2MnO_3{\cdot}(1-x)LiCo_{1/3}Ni_{1/3}Mn_{1/3}O_2$ ($x = 0.1, 0.2, 0.3, 0.4$, and 0.5), respectively.

Magnified XRD patterns between 20° and 25° are given in Fig. 2 inset (left). The peaks observed between 20° and 25° represent the existence of Li_2MnO_3 phase in $LiMO_2$ [15,19,25,26]. The lattice parameters between 20° and 25° match with the ICDD card (No: 98-016-6861) [27]. The small peaks observed at 20.806° (020), 21.556° (110), 24.260° (111) also confirm the existence of monoclinic Li_2MnO_3 with C 2/m space group. In addition, the intensities of the peaks at 20.806° increase slightly while x increases from 0.1 to 0.5, which is an indication of increasing content and/or crystallinity of the Li_2MnO_3 phase in these composites [14,17,19,25].

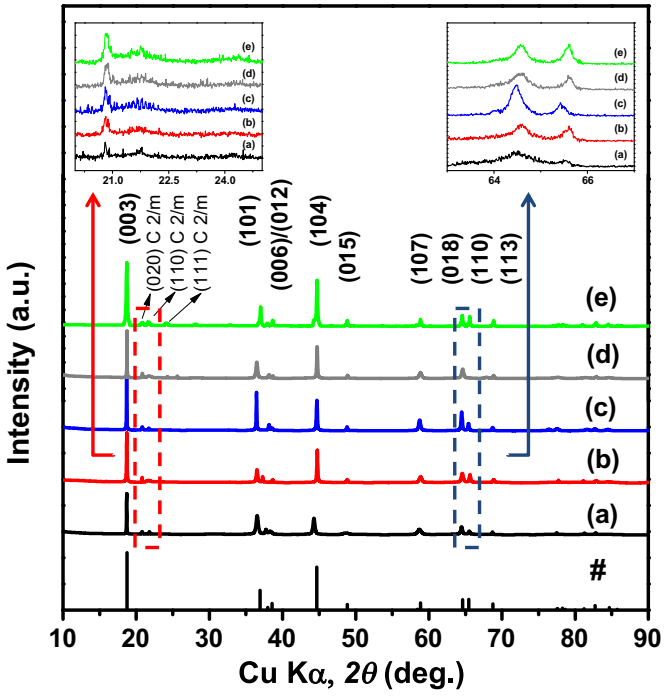

Fig. 2. X-ray diffraction patterns of $xLi_2MnO_3{\cdot}(1-x)LiNi_{1/3}Co_{1/3}Mn_{1/3}O_2$ composites where (a) $x = 0.1$, (b) $x = 0.2$, (c) $x = 0.3$, (d) $x = 0.4$, and (e) $x = 0.5$. The reflections of $LiMn_{1/3}Ni_{1/3}Co_{1/3}O_2$ (ICDD No. 98-016-2294) are shown for comparison [47].

Magnified XRD patterns between 63° and 67° are shown in Fig. 2 inset (right). The intensity and separation of 64.622° (018) and 65.444° (110) peaks are the most noticeable in $0.3Li_2MnO_3{\cdot}0.7LiNi_{1/3}Co_{1/3}Mn_{1/3}O_2$, which may reflect the higher structural order in this particular composite [13–15,17,18,28,29].

The intensity ratio of I_{003}/I_{104} can be used for comparing the cation mixing degree of the layered structure among various composites [30–32]. As reported previously, higher I_{003}/I_{104} value indicates better structural order and a I_{003}/I_{104} value of less than 1.2 reflects the undesirable cation mixing [30–32]. The I_{003}/I_{104} values for $xLi_2MnO_3{\cdot}(1-x)LiNi_{1/3}Co_{1/3}Mn_{1/3}O_2$ ($x = 0.1, 0.2, 0.3, 0.4$ and 0.5) composites are 1.47, 1.53, 1.97, 1.66 and 1.47, respectively. The highest I_{003}/I_{104} value is obtained for $0.3Li_2MnO_3{\cdot}0.7LiMn_{1/3}Ni_{1/3}Co_{1/3}O_2$, indicating this composite has the highest structural order.

Another important parameter related to the order of the material structure is the R factor which is defined as: $(I_{006}+I_{012})/I_{101}$. A lower R value represents better hexagonal order. The R values are 0.77, 0.69, 0.38, 0.53, and 0.76, respectively, for $xLi_2MnO_3{\cdot}(1-x)LiNi_{1/3}Co_{1/3}Mn_{1/3}O_2$ ($x = 0.1, 0.2, 0.3, 0.4$ and 0.5) composites. Among all five composites, $0.3Li_2MnO_3{\cdot}0.7LiNi_{1/3}Co_{1/3}Mn_{1/3}O_2$ gives the lowest R value, indicating a better hexagonal order for this composite [33,34].

These XRD results show that $0.3Li_2MnO_3{\cdot}0.7LiNi_{1/3}Co_{1/3}Mn_{1/3}O_2$ has the optimum composite structure in terms of structural orders.

3.2. Morphology of $xLi_2MnO_3{\cdot}(1-x)LiNi_{1/3}Co_{1/3}Mn_{1/3}O_2$ composites

Fig. 3 shows the SEM images and particle size distributions of $xLi_2MnO_3{\cdot}(1-x)LiCo_{1/3}Ni_{1/3}Mn_{1/3}O_2$ composites. Average particle sizes are determined to be 396, 457, 475, 485 and 699 nm, respectively, for $xLi_2MnO_3{\cdot}(1-x)LiCo_{1/3}Ni_{1/3}Mn_{1/3}O_2$ ($x = 0.1, 0.2, 0.3, 0.4$, and 0.5) composites. The gradual increase in particle size is probably caused by higher viscosities of the corresponding precursor solutions at higher x values. As shown in the magnified inset images, all composites are well-shaped with sharp edges and smooth surfaces. This can also be confirmed by the TEM image (Fig. 4), which shows that $0.3Li_2MnO_3{\cdot}0.7LiCo_{1/3}Ni_{1/3}Mn_{1/3}O_2$ presents well-defined edges with a hexagonal layered structure.

3.3. Electrochemical performance of $xLi_2MnO_3{\cdot}(1-x)LiNi_{1/3}Co_{1/3}Mn_{1/3}O_2$ composites

EIS measurements were carried out in the frequency range from 1 mHz to 1 MHz with an AC voltage signal of ±10 mV for $xLi_2MnO_3{\cdot}(1-x)LiCo_{1/3}Ni_{1/3}Mn_{1/3}O_2$ composites. Prior to the EIS measurements, cells were firstly activated by five cycles at 0.1C between 2 V and 4.8 V vs. Li/Li^+ in order to obtain the stable formation of solid–electrolyte interface (SEI) film on the surface of the cathode [35]. Fig. 5a illustrates the typical Nyquist plot of $0.3Li_2MnO_3{\cdot}0.7LiCo_{1/3}Ni_{1/3}Mn_{1/3}O_2$ composite. The amplifications of the high and medium frequency regions of $xLi_2MnO_3{\cdot}(1-x)LiCo_{1/3}Ni_{1/3}Mn_{1/3}O_2$ composites are shown in Fig. 5b. For a typical EIS curve, the intercept in high frequency to the real axis relates to the ohmic resistance of electrolyte (R_S). The depressed semicircle in medium frequency region is related to the charge transfer resistance (R_{CT}) at the particle surfaces. In general, an increased semicircle radius indicates an increased charge transfer resistance. The straight line in the low frequency region is related to the diffusion behavior of lithium ions within the $xLi_2MnO_3{\cdot}(1-x)LiCo_{1/3}Ni_{1/3}Mn_{1/3}O_2$ particles or also called Warburg resistance (W) [36–40]. The impedance parameters calculated from the EIS curves shown in Fig. 5 is given in Table 2.

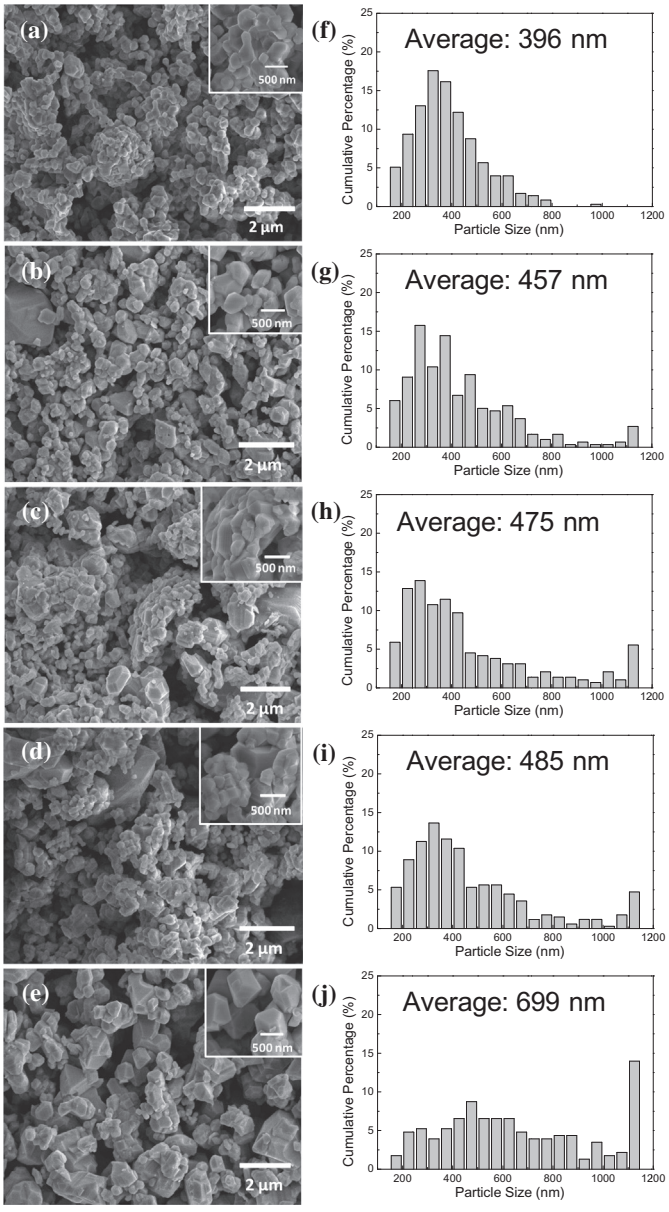

Fig. 3. SEM images and particle size distributions of $xLi_2MnO_3\cdot(1-x)LiNi_{1/3}Co_{1/3}Mn_{1/3}O_2$ composites where (a, f) $x = 0.1$, (b, g) $x = 0.2$, (c, h) $x = 0.3$, (d, i) $x = 0.4$, and (e, j) $x = 0.5$.

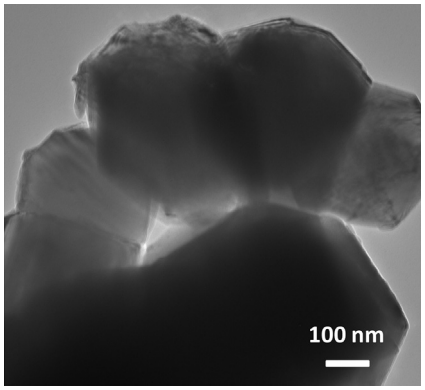

Fig. 4. TEM image of $0.3Li_2MnO_3\cdot0.7LiMn_{1/3}Ni_{1/3}Co_{1/3}O_2$ powder.

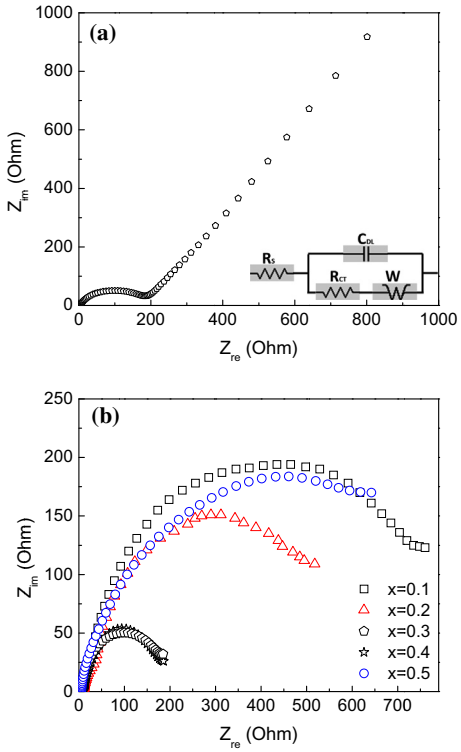

Fig. 5. (a) Typical Nyquist plot of $0.3Li_2MnO_3\cdot0.7LiNi_{1/3}Co_{1/3}Mn_{1/3}O_2$ composite with equivalent circuit model (inset) and (b) impedance spectra of $xLi_2MnO_3\cdot(1-x)LiNi_{1/3}Co_{1/3}Mn_{1/3}O_2$ composites ($x = 0.1$, 0.2, 0.3, 0.4, and 0.5).

From Table 2 and Fig. 5b, it is seen that the charge transfer resistance (R_{CT}) values are 423, 292, 124, 135 and 411 Ω, respectively, for $xLi_2MnO_3\cdot(1-x)LiCo_{1/3}Ni_{1/3}Mn_{1/3}O_2$ ($x = 0.1$, 0.2, 0.3, 0.4, and 0.5) composites. Among all samples, the $0.3Li_2MnO_3\cdot0.7LiCo_{1/3}Ni_{1/3}Mn_{1/3}O_2$ composite has the lowest R_{CT} value, indicating that this composite possesses better reaction kinetics of lithium ion insertion and extraction during electrochemical cycling than other $xLi_2MnO_3\cdot(1-x)LiCo_{1/3}Ni_{1/3}Mn_{1/3}O_2$ ($x = 0.1$, 0.2, 0.4, and 0.5) composites. The reduction of the charge transfer resistance of $0.3Li_2MnO_3\cdot0.7LiCo_{1/3}Ni_{1/3}Mn_{1/3}O_2$ composite can be related to its better structural order which was also aforementioned in Section 3.2 [15,24].

Fig. 6 shows the charge and discharge curves of $xLi_2MnO_3\cdot(1-x)LiNi_{1/3}Co_{1/3}Mn_{1/3}O_2$ composites at a current density of 0.1C in a voltage range of 2–4.6 V. The Li_2MnO_3 content is critical in determining the electrochemical performance of the composites. The initial charge capacities are 136, 250, 292, 308, and 192 mAh g^{-1}, respectively, for $xLi_2MnO_3\cdot(1-x)LiCo_{1/3}Ni_{1/3}Mn_{1/3}O_2$ ($x = 0.1$, 0.2, 0.3, 0.4, and 0.5) composites. Initial discharge capacities are 63, 127, 184, 186, and 85 mAh g^{-1}, respectively. Among all five composites, $0.3Li_2MnO_3\cdot0.7LiCo_{1/3}Ni_{1/}$

Table 2
Impedance parameters of $xLi_2MnO_3\cdot(1-x)LiMn_{1/3}Ni_{1/3}Co_{1/3}O_2$ composites ($x = 0.1$, 0.2, 0.3, 0.4, and 0.5).

Chemical formula	R_S (Ω)	R_{CT} (Ω)	C_{DL} (F)	W (S $s^{0.5}$)
$0.1Li_2MnO_3\cdot0.9LiCo_{1/3}Ni_{1/3}Mn_{1/3}O_2$	11.97	423	$6.08*10^{-5}$	$8.62*10^{-5}$
$0.2Li_2MnO_3\cdot0.8LiCo_{1/3}Ni_{1/3}Mn_{1/3}O_2$	11.75	292	$1.42*10^{-7}$	$1.25*10^{-4}$
$0.3Li_2MnO_3\cdot0.7LiCo_{1/3}Ni_{1/3}Mn_{1/3}O_2$	11.39	124	$8.36*10^{-9}$	$2.25*10^{-2}$
$0.4Li_2MnO_3\cdot0.6LiCo_{1/3}Ni_{1/3}Mn_{1/3}O_2$	11.46	135	$9.54*10^{-8}$	$3.52*10^{-3}$
$0.5Li_2MnO_3\cdot0.5LiCo_{1/3}Ni_{1/3}Mn_{1/3}O_2$	11.89	411	$7.55*10^{-6}$	$7.48*10^{-4}$

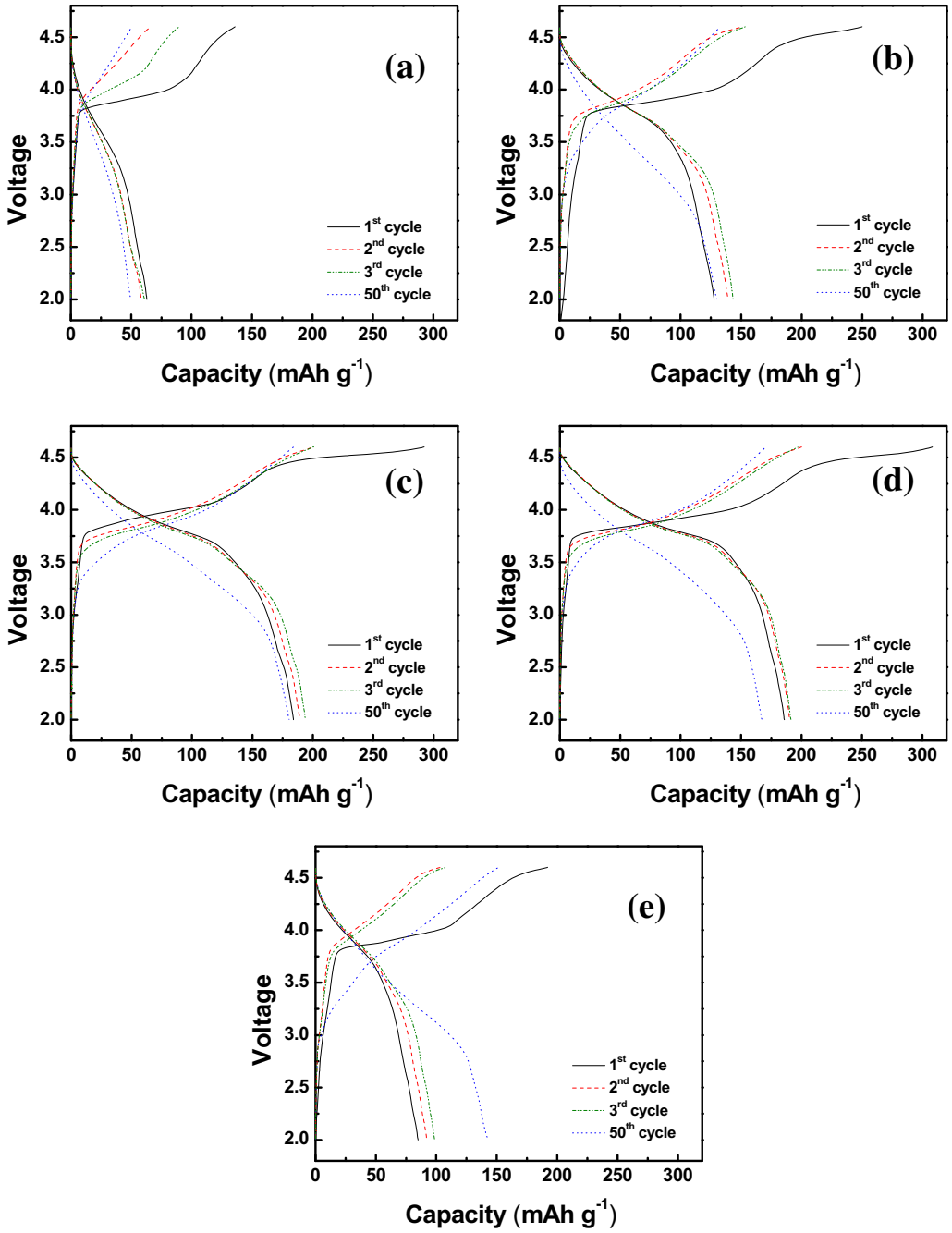

Fig. 6. Galvanostatic charge/discharge curves of $xLi_2MnO_3\cdot(1-x)LiNi_{1/3}Co_{1/3}Mn_{1/3}O_2$ composites where (a) $x = 0.1$, (b) $x = 0.2$, (c) $x = 0.3$, (d) $x = 0.4$, and (e) $x = 0.5$ at 0.1C.

$_3Mn_{1/3}O_2$ and $0.4Li_2MnO_3\cdot0.6LiCo_{1/3}Ni_{1/3}Mn_{1/3}O_2$ show relatively high initial capacities.

From Fig. 6, it is also seen that during charging, $0.3Li_2MnO_3\cdot0.7LiCo_{1/3}Ni_{1/3}Mn_{1/3}O_2$ and $0.4Li_2MnO_3\cdot0.6LiCo_{1/3}Ni_{1/3}Mn_{1/3}O_2$ show a wider plateau region between 3.75 and 4.0 V, as compared with other three composites [17,41]. The electrode reaction between 3.75 and 4.0 V can be written as:

$$LiCo_{1/3}Ni_{1/3}Mn_{1/3}O_2 \rightarrow Li_{1-y}Co_{1/3}Ni_{1/3}Mn_{1/3}O_2 + ye^- + yLi^+ \quad (1)$$

In addition to the plateau between 3.75 and 4.0 V, $0.3Li_2MnO_3\cdot0.7LiCo_{1/3}Ni_{1/3}Mn_{1/3}O_2$ and $0.4Li_2MnO_3\cdot0.6LiCo_{1/3}Ni_{1/3}Mn_{1/3}O_2$ composites also show a second plateau region at around 4.5 V, which can be attributed to the activation of inactive Li_2MnO_3 content in the composites [17,41]. The activation reaction at high potentials was previously given by Thackeray et al. [42] as:

$$Li_2MnO_3 \rightarrow MnO_2 + Li_2O \quad (2)$$

The $0.1Li_2MnO_3\cdot0.9LiCo_{1/3}Ni_{1/3}Mn_{1/3}O_2$ composite does not show the second plateau probably because of the low Li_2MnO_3 content [17], confirmed by the XRD data (see Fig. 2). Although $0.5Li_2MnO_3\cdot0.5LiCo_{1/3}Ni_{1/3}Mn_{1/3}O_2$ has higher amount of Li_2MnO_3 in the structure, the voltage used might not be high enough for the activation of this particular composite [17,43] and a higher-voltage electrolyte might be required to discharge the composite to higher potentials to exhibit the second plateau region. From Fig. 6, another important observation is the irreversible nature of the second

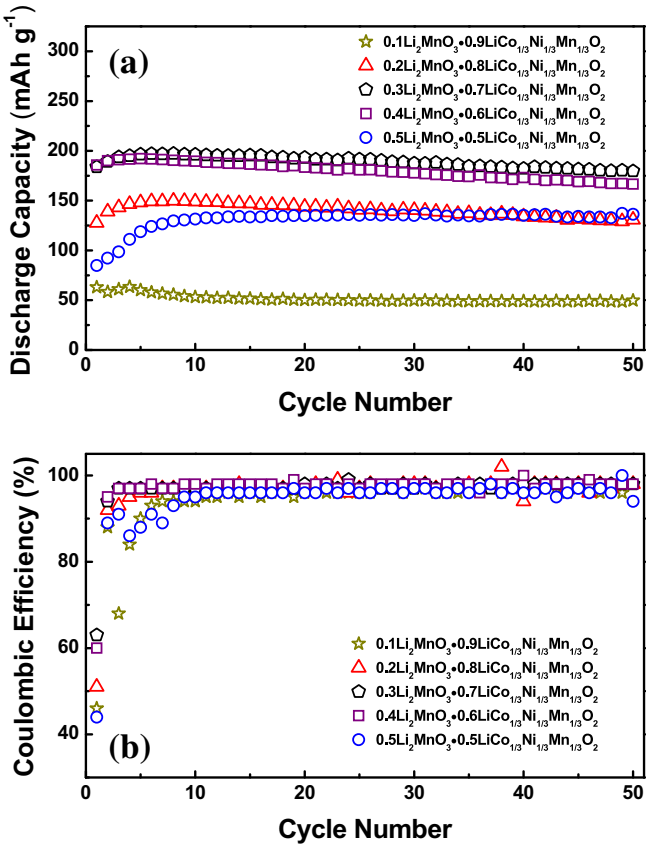

Fig. 7. Cycling performance of $xLi_2MnO_3\cdot(1-x)LiNi_{1/3}Co_{1/3}Mn_{1/3}O_2$ composites. (a) Discharge capacity, and (b) coulombic efficiency.

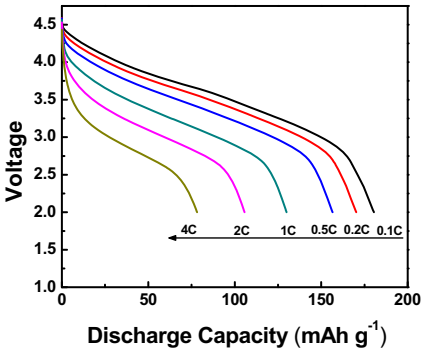

Fig. 8. Initial discharge curves of $0.3Li_2MnO_3\cdot0.7LiMn_{1/3}Ni_{1/3}Co_{1/3}O_2$ under different C-rates.

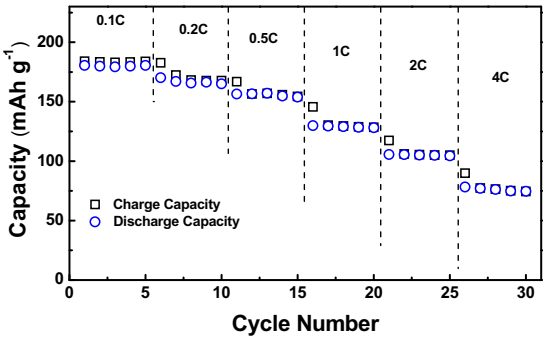

Fig. 9. Rate capability results of $0.3Li_2MnO_3\cdot0.7LiMn_{1/3}Ni_{1/3}Co_{1/3}O_2$.

plateau region after the first cycle. This was reported previously and attributed to the irreversible removal of Li and O from the structure during the activation of L_2MnO_3 [21,43–46].

Fig. 7 shows discharge capacities and corresponding Coulombic efficiencies of $xLi_2MnO_3\cdot(1-x)LiNi_{1/3}Co_{1/3}Mn_{1/3}O_2$ composites for 50 cycles. From Fig. 7a, it can be seen that at the 50th cycle, $xLi_2MnO_3\cdot(1-x)LiCo_{1/3}Ni_{1/3}Mn_{1/3}O_2$ ($x = 0.1$, 0.2, 0.3, 0.4, and 0.5) composites show charge capacities of 51, 133, 184, 171, and 152 mAh g^{-1}, respectively. In addition, except for $0.1Li_2MnO_3\cdot0.9LiCo_{1/3}Ni_{1/3}Mn_{1/3}O_2$, the discharge capacities of the composites increase in the first few cycles, and then keep relatively constant. At the 50th cycle, the capacity retentions are 79.3, 102.3, 89.7, 98.3, and 168%, respectively, for $xLi_2MnO_3\cdot(1-x)LiCo_{1/3}Ni_{1/3}Mn_{1/3}O_2$ ($x = 0.1$, 0.2, 0.3, 0.4, and 0.5) composites. Among all five composites, $0.3Li_2MnO_3\cdot0.7LiCo_{1/3}Ni_{1/3}Mn_{1/3}O_2$ shows the highest capacities in the 50th cycles.

As given in Fig. 7b, the first-cycle Coulombic efficiencies are 46, 52, 65, 62, and 45%, respectively, for $xLi_2MnO_3\cdot(1-x)LiCo_{1/3}Ni_{1/3}Mn_{1/3}O_2$ ($x = 0.1$, 0.2, 0.3, 0.4, and 0.5) composites. It is also obvious that all five composites show Coulombic efficiencies greater than 95% after the first few cycles. From Fig. 7, it can be concluded that among all five composites, $0.3Li_2MnO_3\cdot0.7LiCo_{1/3}Ni_{1/3}Mn_{1/3}O_2$ shows the largest discharge capacity, highest initial Coulombic efficiency, and best capacity retention at the 50th cycle.

The rate capacity performance of $0.3Li_2MnO_3\cdot0.7LiCo_{1/3}Ni_{1/3}Mn_{1/3}O_2$ was determined. Fig. 8 shows the initial discharge curves of $0.3Li_2MnO_3\cdot0.7LiCo_{1/3}Ni_{1/3}Mn_{1/3}O_2$ at various C-rates. It is seen that the discharge curves at different C-rates have the same shape. However, the plateau region is narrower at higher C-rates, which results in reduced discharge capacities. Discharge capacities of $0.3Li_2MnO_3\cdot0.7LiCo_{1/3}Ni_{1/3}Mn_{1/3}O_2$ are determined to be 180, 170, 156, 130, 105, and 78 mAh g^{-1}, respectively, under 0.1, 0.2, 0.5, 1C, 2C, and 4C. The decreased capacities at higher C-rates are caused by the high polarization of the material at high currents [17]. Fig. 9 shows the rate capabilities of $0.3Li_2MnO_3\cdot0.7LiCo_{1/3}Ni_{1/3}Mn_{1/3}O_2$. The composite shows good rate capability when the C-rate increases from 0.1 to 4C. In addition, good cycling performance can observed at each C-rate for 5 cycles.

Based on the results discussed above, it can be concluded that among all five composites, $0.3Li_2MnO_3\cdot0.7LiCo_{1/3}Ni_{1/3}Mn_{1/3}O_2$ shows the highest capacity and best cycling performance. Although the rate capability results are relatively good, they are still inadequate for certain applications such high-power electrical vehicles. This problem is related not only with the cathode structure, but also the electrolyte. To address this issue and enhance the cathode performance, further work is required for the determination of optimum electrolyte systems and the modification of the cathode structure and surface.

4. Conclusions

Various $xLi_2MnO_3\cdot(1-x)LiCo_{1/3}Ni_{1/3}Mn_{1/3}O_2$ ($x = 0.1$, 0.2, 0.3, 0.4, and 0.5) cathode materials have been prepared by a one-step sol–gel route for use in lithium-ion batteries. The morphology, structure and electrochemical performance of the composites were found to be affected by the composite composition. Although all composites showed an α-$NaFeO_2$ structure with R3m space group, the $0.3Li_2MnO_3\cdot0.7LiCo_{1/3}Ni_{1/3}Mn_{1/3}O_2$ composite presented the optimum structural order and the best electrochemical performance. The $0.3Li_2MnO_3\cdot0.7LiCo_{1/3}Ni_{1/3}Mn_{1/3}O_2$ composite showed discharge capacity of 184 mAh g^{-1} at the first cycle and a capacity retention ratio of 98% at the 50th cycle with coulombic efficiencies ranging from 98 to 100% during cycling. Results demonstrated that

the one-step sol–gel process is a promising approach to produce $xLi_2MnO_3 \cdot (1 - x)LiCo_{1/3}Ni_{1/3}Mn_{1/3}O_2$ cathode materials with potentially high performance and low cost.

Acknowledgments

The authors wish to acknowledge the funding from the Advanced Transportation Energy Center and ERC Program of the National Science Foundation under Award Number EEC-08212121. Facilities and resources at the NCSU College of Textiles and the Department of Chemical and Biomolecular Engineering were utilized to complete this research.

References

[1] A. Armstrong, P. Bruce, Nature 381 (1996) 499–500.
[2] J. Tarascon, M. Armand, Nature 414 (2001) 359–367.
[3] M. Whittingham, Chem. Rev. 104 (2004) 4271–4301.
[4] B. Xu, D. Qian, Z. Wang, Y.S. Meng, Mater. Sci. Eng. Res. 73 (2012) 51–65.
[5] C. Delmas, M. Ménétrier, L. Croguennec, I. Saadoune, A. Rougier, C. Pouillerie, G. Prado, M. Grüne, L. Fournès, Electrochim. Acta 45 (1999) 243–253.
[6] P. Kalyani, N. Kalaiselvi, Sci. Technol. Adv. Mater. 6 (2005) 689–703.
[7] S. Schougaard, J. Breger, M. Jiang, C. Grey, J. Goodenough, Adv. Mater. 18 (2006) 905.
[8] K.M. Shaju, P.G. Bruce, Adv. Mater. 18 (2006) 2330.
[9] J. Kim, H. Chung, Electrochim. Acta 49 (2004) 3573–3580.
[10] T. Ohzuku, K. Ariyoshi, S. Yamamoto, Y. Makimura, Chem. Lett. (2001) 1270–1271.
[11] Z. Lu, D. MacNeil, J. Dahn, Electrochem. Solid State Lett. 4 (2001) A200–A203.
[12] S. Kang, P. Kempgens, S. Greenbaum, A.J. Kropf, K. Amine, M.M. Thackeray, J. Mater. Chem. 17 (2007) 2069–2077.
[13] D. Kim, J. Gim, J. Lim, S. Park, J. Kim, Mater. Res. Bull. 45 (2010) 252–255.
[14] S. Kim, C. Kim, J. Noh, S. Yu, S. Kim, W. Chang, W.C. Choi, K.Y. Chung, B. Cho, J. Power Sources 220 (2012) 422–429.
[15] J. Lim, H. Bang, K. Lee, K. Amine, Y. Sun, J. Power Sources 189 (2009) 571–575.
[16] M.M. Thackeray, S. Kang, C.S. Johnson, J.T. Vaughey, R. Benedek, S.A. Hackney, J. Mater. Chem. 17 (2007) 3112.
[17] C. Yu, X. Guan, G. Li, J. Zheng, L. Li, Script. Mater. 66 (2012) 300–303.
[18] C. Yu, G. Li, X. Guan, J. Zheng, L. Li, T. Chen, Electrochim. Acta 81 (2012) 283.
[19] L. Yu, W. Qiu, J. Huang, F. Lian, Int. J. Miner. Metall. Mater. 16 (2009) 458–462.
[20] Z. Chen, Y. Sun, K. Amine, J. Electrochem. Soc. 153 (2006) A1818–A1822.
[21] Z. Lu, J. Dahn, J. Electrochem. Soc. 149 (2002) A815–A822.
[22] N. Choi, Z. Chen, S.A. Freunberger, X. Ji, Y. Sun, K. Amine, G. Yushin, L.F. Nazar, J. Cho, P.G. Bruce, Angew. Chem. Int. Ed. 51 (2012) 9994–10024.
[23] H. Deng, I. Belharouak, Y. Sun, K. Amine, J. Mater. Chem. 19 (2009) 4510.
[24] C. Yu, H. Wang, X. Guan, J. Zheng, L. Li, J. Alloys Compd. 546 (2013) 239–245.
[25] J. Kim, C. Park, Y. Sun, Solid State Ionics 164 (2003) 43–49.
[26] C.S. Johnson, N. Li, C. Lefief, M.M. Thackeray, Electrochem. Commun. 9 (2007) 787–795.
[27] A. Boulineau, L. Croguennec, C. Delmas, F. Weill, Solid State Ionics 180 (2010) 1652–1659.
[28] J. Li, R. Kloepsch, M.C. Stan, S. Nowak, M. Kunze, M. Winter, S. Passerini, J. Power Sources 196 (2011) 4821–4825.
[29] Z. Zhong, N. Ye, H. Wang, Z. Ma, Chem. Eng. J. 175 (2011) 579–584.
[30] B. Hwang, R. Santhanam, C. Chen, J. Power Sources 114 (2003) 244–252.
[31] R. Alcantara, P. Lavela, J. Tirado, R. Stoyanova, E. Zhecheva, J. Electrochem. Soc. 145 (1998) 730–736.
[32] Z. Chang, Z. Chen, F. Wu, H. Tang, Z. Zhu, X.Z. Yuan, H. Wang, Electrochim. Acta 53 (2008) 5927–5933.
[33] S.J. Shi, J.P. Tu, Y.Y. Tang, Y.X. Yu, Y.Q. Zhang, X.L. Wang, J. Power Sources 221 (2013) 300.
[34] J. Wang, M. Zhang, C. Tang, Y. Xia, Z. Liu, Electrochim. Acta 80 (2012) 15–21.
[35] G.X. Wang, L. Yang, Y. Chen, J.Z. Wang, S. Bewlay, H.K. Liu, Electrochim. Acta 50 (2005) 4649–4654.
[36] F. Gao, Z. Tang, Electrochim. Acta 53 (2008) 5071–5075.
[37] H. Liu, C. Li, H.P. Zhang, L.J. Fu, Y.P. Wu, H.Q. Wu, J. Power Sources 159 (2006) 717–720.
[38] C.K. Park, S.B. Park, H.C. Shin, W.I. Cho, H. Jang, Bull. Korean Chem. Soc. 32 (2011) 191–195.
[39] C. Chang, L. Her, H. Su, S. Hsu, Y.T. Yen, J. Electrochem. Soc. 158 (2011) A481–A486.
[40] O. Toprakci, H.A.K. Toprakci, L. Ji, G. Xu, Z. Lin, X. Zhang, ACS Appl. Mater. Interfaces 4 (2012) 1273–1280.
[41] Z.Q. Deng, A. Manthiram, J. Phys. Chem. C 115 (2011) 7097–7103.
[42] M.M. Thackeray, C.S. Johnson, J.T. Vaughey, N. Li, S.A. Hackney, J. Mater. Chem. 15 (2005) 2257.
[43] Q. Peng, Z. Tang, L. Zhang, X. Li, Mater. Res. Bull. 44 (2009) 2147–2151.
[44] A. Robertson, P. Bruce, Electrochem. Solid State Lett. 7 (2004) A294–A298.
[45] A. Armstrong, M. Holzapfel, P. Novak, C. Johnson, S. Kang, M. Thackeray, P. Bruce, J. Am. Chem. Soc. 128 (2006) 8694–8698.
[46] N. Yabuuchi, K. Yoshii, S. Myung, I. Nakai, S. Komaba, J. Am. Chem. Soc. 133 (2011) 4404–4419.
[47] E. Shinova, R. Stoyanova, E. Zhecheva, G.F. Ortiz, P. Lavela, J.L. Tirado, Solid State Ionics 179 (2008) 2198–2208.